Femtosecond photoelectron diffraction: a new approach to image molecular structure during photochemical reactions

Daniel Rolles*[a], Rebecca Boll[a,b], Samyak R. Tamrakar[a,c], Denis Anielski[a,b], Cédric Bomme[a]

[a]Deutsches Elektronen-Synchrotron (DESY), Notkestraβe 85, 22607 Hamburg, Germany; [b]Max-Planck-Institut für Kernphysik, Am Saupfercheckweg 1, 69117 Heidelberg, Germany; [c]Jacobs Universität Bremen, Campus Ring 1, 28759 Bremen, Germany

ABSTRACT

Continuing technical advances in the creation of (sub-) femtosecond VUV and X-ray pulses with Free-Electron Lasers and laser-based high-harmonic-generation sources have created new opportunities for studying ultrafast dynamics during chemical reactions. Here, we present an approach to image the geometric structure of gas-phase molecules with few-femtosecond temporal and sub-Ångström spatial resolution using femtosecond photoelectron diffraction. This technique allows imaging the molecules "from within" by analyzing the diffraction of inner-shell photoelectrons that are created by femtosecond VUV and X-ray pulses. Using pump-probe schemes, ultrafast structural changes during photochemical reactions can thus be directly visualized with a temporal resolution that is only limited by the pulse durations of the pump and the probe pulse and the synchronization of the two light pulses. Here, we illustrate the principle of photoelectron diffraction using a simple, geometric scattering model and present results from photoelectron diffraction experiments on laser-aligned molecules using X-ray pulses from a Free-Electron Laser.

Keywords: photoelectron diffraction, photoelectron holography, ultrafast dynamics, gas-phase molecules, Free-Electron Laser, molecular-frame photoelectron angular distribution, velocity map imaging, photoelectron imaging

1. INTRODUCTION

Diffraction methods such as X-ray and electron diffraction are powerful tools for structure determination that have contributed significantly to our knowledge of the microscopic structure of matter. A somewhat lesser-known member of the family of diffraction techniques is photoelectron diffraction (PD; sometimes also referred to as X-ray photoelectron diffraction, XPD)[1,2,3,45], in which X-ray photons are used to emit an inner-shell photoelectron from a specific atom inside a molecule or a solid, and the scattering and diffraction of this photoelectron encodes the structural information on the environment of the emitter atom. PD is used, in particular, in condensed matter and surface physics applications, e.g., to determine the geometry of surface reconstructions or of adsorbate atoms or molecules on a surface[1,2,3]. Two-dimensional PD images can even be interpreted as photoelectron holograms, which allows direct holographic reconstruction of the geometric structure without the need of phase-retrieval methods or further modeling[1,4].

Although it was recognized a long time ago that photoelectron diffraction effects could, under certain conditions, also be observed in gas-phase molecules, e.g. by recording molecular-frame photoelectron angular distributions (MFPADs)[5,6,7,8], PD has not played a major role in gas-phase studies to date since far more precise methods, such as microwave spectroscopy, exist to determine the ground-state geometry of molecules in the gas phase. However, with the increased interest in recent years in studying non-equilibrium structures such as reaction intermediates and other transient species, and with new experimental developments that allow studying these structures on ultrafast time scales using femtosecond-lasers, laser-based high harmonic generation (HHG) sources, and Free-Electron Lasers (FELs), this situation may change since femtosecond photoelectron diffraction (fs-PD)[9,10,11,12,13] may allow accessing time-resolved structural information on transient states that is not accessible by other, conventional methods of structure determination.

---

*Daniel.Rolles@desy.de

In this paper, we report our recent progress towards developing fs-PD as a method for imaging the geometric structure of gas-phase molecules with few-femtosecond temporal and sub-Ångström spatial resolution. We begin by illustrating the principle of PD and the relationship between photoelectron diffraction and molecular-frame photoelectron angular distributions (MFPADs) using a simple, geometric scattering model. We then present recent experiments aiming at developing the experimental capabilities for recording time-resolved photoelectron diffraction images using femtosecond X-ray pulses from Free-Electron Lasers, and conclude by summarizing advantages and challenges of the fs-PD method for gas-phase molecules as well as by pointing out possible future improvements.

2. A SIMPLE MODEL OF PHOTOELECTRON DIFFRACTION IN MOLECULES

A photoelectron diffraction pattern is created by the superposition of direct and scattered photoelectron waves, leading to constructive or destructive interference that result in angle- and energy-dependent intensity variations at the position of the photoelectron detector[1,2,3,4]. The simplest possible scenario of photoelectron diffraction is illustrated in Fig. 1 for the case of a diatomic molecule. When an X-ray photon is absorbed at the core level of a specific atom inside a molecule, in this case the atom A, a coherent photoelectron wave is emitted from a localized origin into the full 4π solid angle. Intra-molecular scattering of the photoelectron wave on the other atom(s) in the molecule then results in additional waves, which, in the simplest possible model of point-like atomic scatterers, each have a phase shift with respect to the original wave that depends only on the geometric path length difference Δs. In particular, no additional scattering phase shifts or angle-dependent scattering amplitudes are taken into account in this simple model.
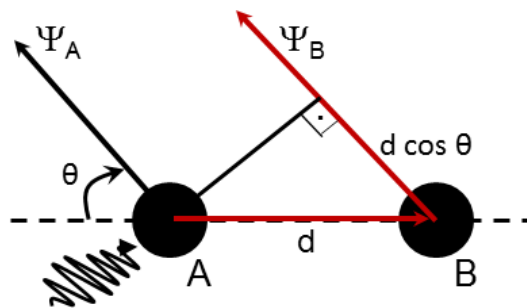

Figure 1. Principle of photoelectron diffraction: A localized electron wave Ψ_A is created by X-ray absorption at a core level of atom A inside the molecule with bond length d. The electron can undergo intra-molecular scattering on other atom(s) within the molecule, resulting, in this case, in one additional scattered wave Ψ_B. In the far field, the interference between direct and scattered waves results in a structured angular pattern $I(\theta) = |\Psi_A + \Psi_B|^2$, which is recorded, e.g., on an electron imaging detector. It can be interpreted as a photoelectron diffraction pattern that contains the information on the molecular structure.

In close analogy to the well-known double-slit interference, constructive interference between the direct and the scattered wave arises for scattering angles θ, for which the path length difference Δs is equal to an integer multiple of the electron de Broglie wavelength λ. However, in contrast to the traditional double-slit scenario, the photoelectron emitted from atom A has to first travel the distance d before scattering on the neighboring atom B, and the total path length difference is thus given by

$$\Delta s = d + d\cos\theta. \qquad (1)$$

In other words, the largest path length difference $\Delta s = 2d$ occurs at $0°$, i.e., in the backscattering direction *away* from the scatterer and towards the emitter atom, while the path length difference is $\Delta s = d$ at $90°$, i.e. perpendicular to the molecular axis. At $180°$, i.e. for emission *towards* the neighboring atom, the path length difference is $\Delta s = 0$. When neglecting multiple scattering effects, an interference maximum commonly referred to as forward scattering peak occurs in this direction independent of the photoelectron wavelength.

The electron's de Broglie wavelength λ is a function of the photoelectron kinetic energy E_{kin} and is given by

$$\lambda = \frac{h}{p} = \frac{h}{\sqrt{2E_{kin}m_e}}.$$ (2)

Here, h is the Planck's constant, p is the nonrelativistic electron momentum, and m_e is the electron mass. In commonly used units, this corresponds to

$$\lambda\ [\mathring{A}] = \frac{12.26}{\sqrt{E_{kin}[eV]}}.$$ (3)

When assuming spherical waves $\Psi \propto e^{i(kr-wt)}/r$ for both the direct and the scattered photoelectron waves, the final photoelectron intensity $I(\theta) = |\Psi_A + \Psi_B|^2$ in the far field, which results from the interference between the direct and the single-scattered wave as shown in Fig. 1 for the case of a diatomic molecule, only depends on the phase difference $\delta(\theta)$ between the two waves. It can be calculated as a function of the scattering angle θ by the simple formula

$$I(\theta) \propto |A + B\,e^{i\delta(\theta)}|^2 = |A + B\,[cos\,\delta(\theta) + i\,sin\,\delta(\theta)\,]|^2.$$ (4)

Here, the coefficients A and B are proportional to the amplitudes of the direct and scattered waves Ψ_A and Ψ_B, respectively. In the spirit of developing the simplest possible model, A and B can be assumed to be proportional to the atomic photoionization cross section of atom A and the elastic electron scattering cross section for atom B, respectively, which can be taken from standard databases[43]. The phase difference δ between the two waves is, using eq. (1), given by

$$\delta(\theta) = \frac{2\pi}{\lambda}\,\Delta s = \frac{2\pi d}{\lambda}\,(1 + cos\,\theta).$$ (5)

Furthermore, we can assume that for the case of photoionization of an inner-shell s-level, the directly emitted photoelectron wave can be described by a pure p-wave along the polarization vector $\boldsymbol{\varepsilon}$. If the photoelectron intensity is considered within the plane defined by the molecular axis and the polarization vector, this p-wave character of the direct wave can be taken into account by simply introducing two additional factors in eq. (4):

$$I_\alpha(\theta) = |A\,cos\,(\theta - \alpha) - B\,cos\alpha\,[cos\,\delta(\theta) + i\,sin\,\delta(\theta)\,]|^2.$$ (6)

The term $cos\,(\theta - \alpha)$ describes the angle-dependent amplitude of the direct p-wave, where α is the angle between the molecular axis and the polarization vector $\boldsymbol{\varepsilon}$, and the term $cos\,\alpha$ decreases the amplitude of the spherical scattered wave accordingly.

When considering detection angles out of the plane or, in particular, for the more general case of a non-cylindrically symmetric, polyatomic molecule, an analogous formula for the angle-dependent photoelectron intensity $I(\phi,\theta)$ can be derived by expressing the direct and scattered waves in terms of spherical harmonics:

$$I(\theta,\phi) = |A\,Y_1^0(\theta,\phi) + \sum_n B_n\,Y_1^0(\Theta_n,\Phi_n)\ Y_0^0(\theta,\phi)\ e^{i\delta(\theta,\phi,d_n,\Theta_n,\Phi_n)}|^2$$ (7)

Here, θ and ϕ are the polar and azimuthal electron emission angles in spherical coordinates with the emitter atom located at the origin of the coordinate system and the molecular reference axis along the z-axis. Θ_n and Φ_n are the coordinates of the other atoms inside the molecule, and Y_l^m are spherical harmonics, where $Y_1^0(\theta,\phi)$ describes a directly emitted p-wave along the z-axis[$], $Y_0^0(\theta,\phi)$ the spherical scattered wave created on atom n, and $Y_1^0(\Theta_n,\Phi_n)$ the intensity of the direct p-wave at the position of atom n. The coefficients B_n scale with $1/d_n$, where d_n is the distance of atom n to the emitter atom.

Footnote: [$]If the polarization vector $\boldsymbol{\varepsilon}$ is along the x or y axis, the spherical harmonics $Y_1^1(\theta,\phi)$ and $Y_1^{-1}(\theta,\phi)$ have to be used instead of $Y_1^0(\theta,\phi)$. For arbitrary polarization angles, a linear combination of the three can be employed.

In analogy to eq. (5), the phase shift δ is given by

$$\delta(\theta,\phi,d_n,\Theta_n,\Phi_n) = \frac{2\pi}{\lambda}\Delta s = \frac{2\pi d_n}{\lambda}\left[1 - \begin{pmatrix} \sin\Theta_n\cos\Phi_n \\ \sin\Theta_n\sin\Phi_n \\ \cos\Theta_n \end{pmatrix}\begin{pmatrix} \sin\theta\cos\phi \\ \sin\theta\sin\phi \\ \cos\theta \end{pmatrix}\right]. \qquad (8)$$

Note that eq (7) simplifies to eq. (6) for the special case of a diatomic due to the cylindrical symmetry of the molecule.

Using eq. (6) and (7), we can now calculate, within this simple, point-like geometric single-scattering model, the photoelectron diffraction patterns for two exemplary molecules, CO and CH_3F, as shown in Fig. 2 and Fig. 3.
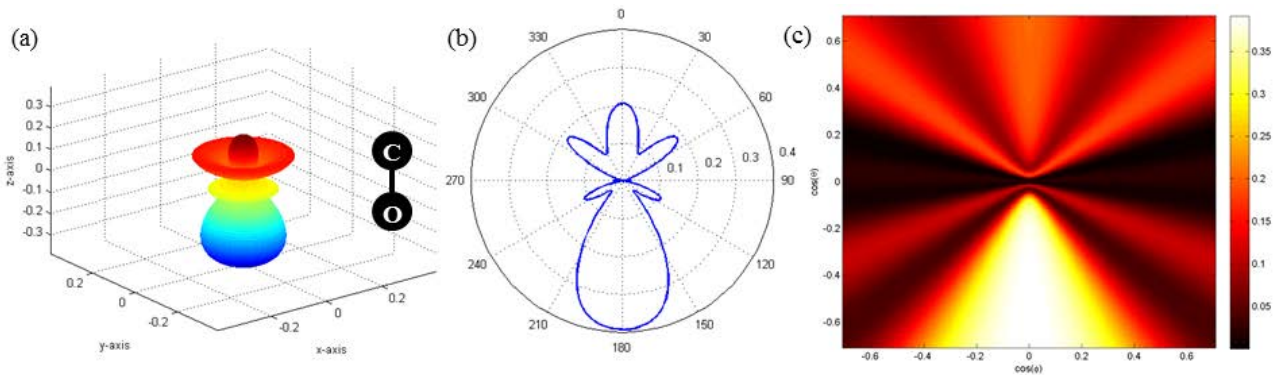

Figure 2. Photoelectron diffraction pattern for C(1s) photoelectron emission from CO molecules at 300 eV photoelectron kinetic energy and for ionization with linearly polarized X-rays with the polarization vector along the molecular axis, which is along the z-axis. (a) Full three-dimensional photoelectron angular distributions. (b) Polar plot of the photoelectron intensity in the xz-plane as a function of the emission angle θ. (c) Two-dimensional (2D) projection of the photoelectron angular distribution onto the xz-plane as it would be recorded by a 2D imaging detector placed parallel to the molecular axis in the far field. For this model calculation, the amplitudes A and B in eq. (4) are assumed to be A=B=1.

Of course, our simple model based on single scattering on point-like scatterers at the position of the atomic constituents in the molecule - instead of taking into account multiple scattering on the full, non-spherical molecular potential - will, in most cases, not be able to quantitatively predict the actual, experimental diffraction patterns, and our examples shown here are thus meant primarily as a qualitative and intuitive way of illustrating the photoelectron diffractions effects. Nevertheless, we would like to point out that the assumption of single scattering and point-like scatterers becomes increasingly justified for increasing photoelectron kinetic energies. We have found that already for electron kinetic energies of a few hundred eV, the diffraction patterns calculated from our simple, point-like geometric single-scattering model agree well with those calculated within a more sophisticated single scattering model that takes into account element and energy-dependent scattering amplitudes[9] and even with those obtained from state-of-the-art DFT calculations[15]. A more systematic comparison between the calculated diffraction patterns obtained from these different models as well as from various multiple-scattering calculations[15,16,17] is currently in progress and will be reported at a later time.
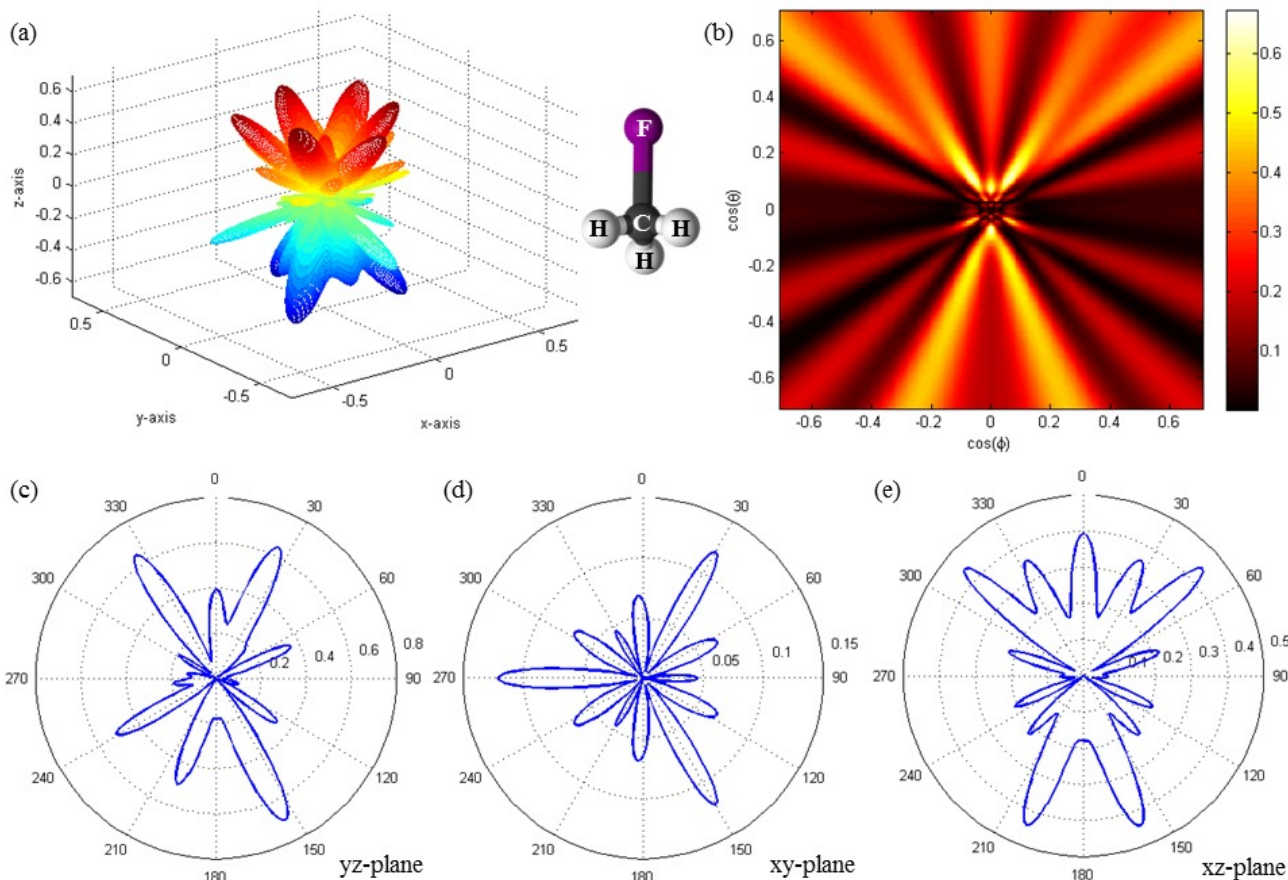
Figure 3. Photoelectron diffraction pattern for F(1*s*) photoelectron emission from CH_3F molecules at 300 eV photoelectron kinetic energy and for ionization with linearly polarized X-rays with the polarization vector along the C-F axis, which is along the z-axis. One of the hydrogen atoms is placed in the yz-plane. (a) Full three-dimensional photoelectron angular distributions. (b) Two-dimensional (2D) projection of the photoelectron angular distribution onto the xz-plane as it would be recorded by a 2D imaging detector placed parallel to the C-F axis in the far field. (c,d,e) Polar plots of the photoelectron intensity in (a) the yz-plane, (d) the yz-plane, and (e) the xz-plane. For this model calculation, the coefficient B_C of the scattered wave originating from the C atom and the coefficients B_H of the scattered waves originating from the H atoms in eq. (7) are chosen to be $B_C=B_H=A=1$ in order to emphasize the interference effects. For $B_C<1$ and $B_H<1$, the contrast between interference maxima and minima is reduced.

3. TIME-RESOLVED PHOTOELECTRON DIFFRACTION EXPERIMENTS WITH FREE-ELECTRON LASERS

In our conceptual discussion of molecular photoelectron diffraction in section 2, we have implicitly and tacitly assumed that the angular dependence of the photoelectron intensity can be determined in the molecular reference frame, i.e. as a function of emission angle with respect to both the light polarization direction and the molecular axis. While this may naturally be the case for molecules on a surface, which often have a clearly defined adsorbate geometry, gas-phase molecules are usually randomly oriented in space, such that most of the angle-dependent interference structure in the photoelectron angular distributions is completely averaged out. In order to observe photoelectron diffraction patterns from gas-phase molecules and to extract structural information, e.g. by holographic reconstruction, from the photoelectron angular distributions, one therefore needs to "fix the molecule in space". This is typically done either by means of angle-resolved photoelectron-ion coincidences[5,6,7,8,18,44], which allows determining the orientation of suitable molecular axis at the time of the photoionization for each individual molecule from the emission directions of the fragment ions, or by actively aligning the molecules in space, e.g. by laser alignment techniques[19]. While we are

pursuing both experimental approaches for our photoelectron diffraction studies, we will concentrate, in the following, on describing our experiments on adiabatically laser-aligned molecules, which we have performed at the Free-Electron Lasers LCLS at SLAC and FLASH at DESY in Hamburg. The experimental setup is described in detail in previous publications[10,11] and is therefore only briefly summarized here. A beam of rotationally cold molecules, typically seeded in helium, is created by supersonic expansion into vacuum through a pulsed Even-Lavie nozzle. It is then crossed with two focused laser beams as well as with an X-ray beam inside a double-sided velocity map imaging (VMI) spectrometer equipped with two MCP detectors with phosphor screens[10,11,20]. The pulses of an injection-seeded Nd:YAG laser (1064 nm, 10ns, ~500 mJ), adiabatically align the molecules along the laser polarization direction. A second laser pulse from a femtosecond Ti:Sapphire laser (266/400/800 nm, ~80 fs, < 1 mJ) initiates a photochemical reaction, e.g. a photodissociation or isomerization, which is subsequently probed, at various time-delays, by photoelectron diffraction using VUV or X-ray Free-Electron Laser pulses (50-2000 eV, 3-80 fs, 0.1-3 mJ). The FEL pulses ionize the aligned molecules by emitting photoelectrons predominantly from a targeted inner-shell level of a specific atom in the molecule. These photoelectrons are then imaged shot-by-shot on one side of the VMI spectrometer, while the resulting fragment ions are simultaneously imaged on the other side of the spectrometer, such that the degree of molecular alignment can be constantly monitored [10,12].

Typical VMI images for F^+ fragment ions and $F(1s)$ photoelectrons resulting from the photoionization of laser-aligned 1-ethynyl-4-fluorobenzene (C_8H_5F, pFAB) molecules at LCLS are shown in Fig. 4. Assuming that the energetic F^+ ions, which result from a Coulomb explosion of the core-ionized pFAB molecule after Auger decay are emitted along the axis of the F-C bond, the angular distribution of these F^+ ions can be used as a quantitative measure for the degree of molecular alignment achieved in the experiment. This is usually done by calculating the expectation value $<cos^2 \theta_{2D}>$, where θ_{2D} is the angle between the momentum vector of the F^+ ion, projected onto the detector plane, and the polarization direction of the YAG laser pulse[19]. For the image shown here, this yields a value of $<cos^2 \theta_{2D} > = 0.89$, indicating that the molecules probed by the FEL pulses are very well aligned.
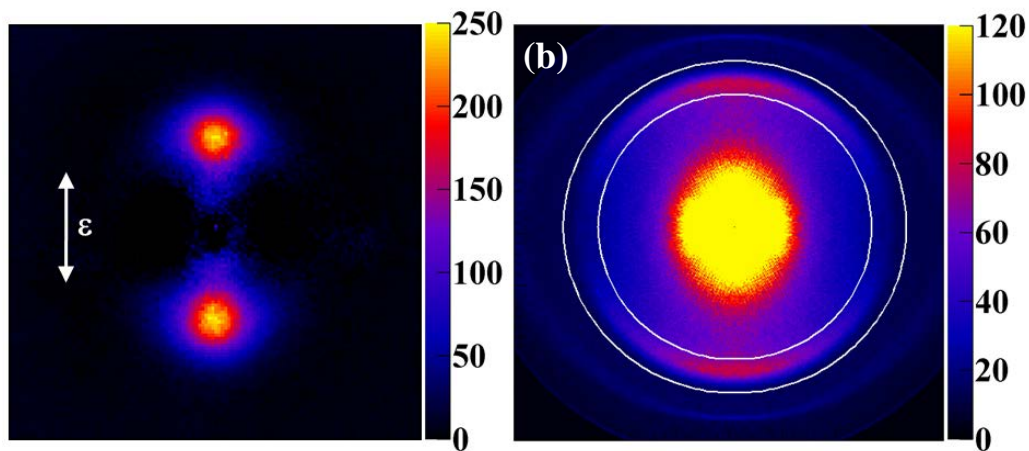

Figure 4.   (a) F^+ ion images from adiabatically laser-aligned pFAB molecules recorded after ionization with linearly polarized X-rays at 723 eV photon energy. The YAG laser pulse was linearly polarized parallel to the FEL polarization as indicated by the white arrow. (b) Electron images recorded simultaneously to the ion image shown in (a). At this photon energy, the $F(1s)$ photoelectrons (marked by the two white circles) have a kinetic energy of 31 eV. Both ion and electron images were obtained by summing the single-shot CCD camera images after using a peak-finding algorithm.

In the corresponding photoelectron image recorded simultaneously with the F^+ ion image on the opposite side of the double-sided VMI spectrometer, the $F(1s)$ photoelectron line with a kinetic energy of 31 eV appears as a ring close to the outer edge of the MCP detector. It is marked by two white circles in Fig. 4 (b). A strong angular anisotropy of the photoelectron intensity reminiscent of the p-wave character of an atomic s-level photoemission can clearly be observed, as well as an intense contribution from lower-energy electrons in the center of the image (see Ref. 11 and 12 for further discussion of these low-energy electrons). Contrary to the expectation based on our photoelectron diffraction model presented in section 2, no clear angular structure apart from the p-wave-like anisotropy is visible in the photoelectron intensity. However, as shown in our previous work[10,12], this is mostly the result of the angular averaging due to the

imperfect molecular alignment, which averages out most of the interference structure despite the relatively high degree of alignment that was achieved in the experiment.

In order to extract the remaining, weak interference effects in the photoelectron images, we subtract the electron images recorded without YAG pulses from those recorded with YAG pulses present[10,12]. The resulting photoelectron angular distribution differences (ΔPADs) for different photoelectron kinetic energies are shown as polar plots in Fig. 5. The experimental data obtained by integrating the difference images over the region of interest marked by the white circles in Fig. 4(b) are shown as dots, while the experimental ΔPADs obtained by subtracting the electron images after inversion with the pBasex algorithm[46] are shown as shaded areas. Both agree well with each other as well as with the results of DFT calculations that take into account the angular averaging due to the molecular alignment (for further details, please refer to our previous publications[10,12]).
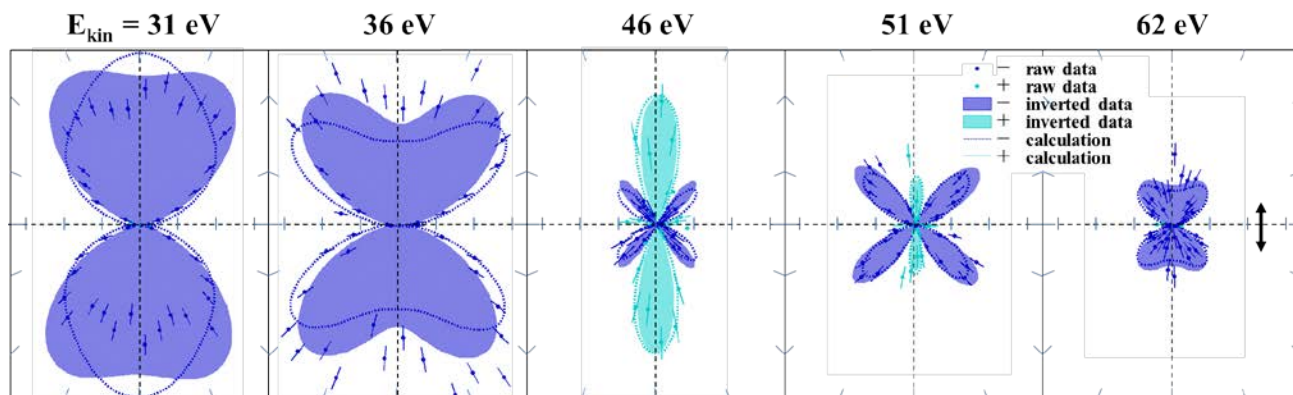

Figure 5. F(1s) photoelectron angular distribution differences (ΔPADs) of pFAB for different photoelectron kinetic energies. Raw data are shown as dots, inverted data as shaded areas, and calculated ΔPADs as lines (blue: negative difference; cyan: positive difference). All distributions are plotted on the same radial axis. Figure taken, with permission, from Ref. 10. *Copyright (2013) by the American Physical Society.*

A clear angular interference structure can be observed in these ΔPADs, which strongly depends on the photoelectron kinetic energy and thus the photoelectron wavelength, as also confirmed by the DFT calculations. However, since simple, single-scattering models are not appropriate at these relatively low photoelectron kinetic energies, it is very challenging to directly relate the measured ΔPADs to the molecular structure without the help of elaborate calculations. Nevertheless, our results still demonstrate the experimental feasibility of photoelectron diffraction experiments on laser-aligned molecules at FELs, and we are planning to perform follow-up experiments at higher kinetic energies and with further experimental improvements, as discussed in the following section, in the near future.

4. CONCLUSIONS AND OUTLOOK

In this paper, we have outlined a simple, geometric scattering model to illustrate the concept of photoelectron diffraction in gas-phase molecules, and presented experimental results from the first realizations of such experiments at a Free-Electron Laser. This work is part of our larger-scale photoelectron diffraction and holography effort, whose aim it is to investigate the feasibility of time-resolved photoelectron diffraction experiments at FELs and to develop and establish this technique as a versatile method for ultrafast studies of chemical reactions in gas-phase molecules. During our first FEL beamtimes at LCLS and FLASH, we have been able to demonstrate several important steps towards this goal. In particular, we have shown that

1. it is possible to measure photoelectron angular distributions of laser-aligned molecules with the currently operating FELs despite the obvious limitations concerning photon energy bandwidth, beam stability, and the very limited setup and measurement time that is available for each experiment;

2. these photoelectron angular distributions are sensitive to changes in the electron wavelength, as shown in Fig. 5 and as expected from diffraction considerations. In particular, we note that decreasing the electron wavelength is expected to change the diffraction pattern in a very similar way as increasing all internuclear distances in the molecule, e.g. in a Coulomb exploding molecule;

3. we can also perform these experiments in a femtosecond pump-probe arrangement and that we can observe changes in the electron images as a function of the pump-probe delay between Ti:Sapphire laser and X-ray pulses[11,12].

Taking advantage of present and future experimental and theoretical improvements, some of which will be discussed below, femtosecond photoelectron diffraction has the potential to become a powerful method for time-resolved studies of gas-phase molecules that is complementary to other methods such as time-resolved X-ray diffraction, ultrafast electron diffraction, and other related techniques such as laser-induced electron diffraction[22,23], which are also of high current interest in the ultrafast imaging community. While X-ray diffraction has been tremendously successful for crystallizable molecules, it has, so far, been difficult to implement even for non-time-resolved studies of individual, small molecules in the gas phase[24,25]. The biggest challenge in imaging molecules with light atomic constituents like carbon or even hydrogen is the very low cross section for the interaction of an energetic X-ray photon with a single atom. This cross section is largely dominated by photoabsorption, resulting in a loss of the X-ray photon for imaging purposes and in unwanted radiation damage. Photoelectron diffraction turns this drawback into a benefit by exploiting the photoelectrons for imaging purposes.

Being an all-optical method for both pump and probe, time-resolved photoelectron diffraction also avoids the problem of velocity mismatch that has, to date, limited the temporal resolution of electron diffraction experiments on gas-phase targets to > 850 fs[26,27]. Finally, by exploiting single-photon ionization and photoemission of inner-shell electrons, fs-PD can be rather well described by simple atomistic models and does not rely on extensive prior knowledge of the geometric structure of the molecules. In particular, contrary to most X-ray or electron (beam) diffraction patterns, which are typically recorded outside of the direct beam, photoelectron diffraction patterns can always be treated as holograms in the sense of Gabor[28]. In this *inside-source* holography arrangement, the phase information is preserved and structural information such as bond lengths and bond angles can be directly extracted from the recorded diffraction signal without complicated phase-retrieval methods and without comparison to modeling calculations[4,9,28,29]. This makes femtosecond photoelectron diffraction and femtosecond photoelectron holography a potentially powerful method to directly image the changing molecular structure during ultrafast chemical reactions, as demonstrated conceptually by Krasniqi *et al.*[9].

However, apart from these intriguing advantages, there are also a number of conceptual and experimental difficulties, which need to be addressed in order to make fs-PD a tool with wide applicability in gas-phase studies:

(i) The photoionization process, which lies at the heart of the photoelectron diffraction method, is considerably more difficult to describe theoretically than the scattering of plane waves in the case of X-ray and electron diffraction. In particular, the distinct angular emission characteristics of photoelectrons (which, in case photoemission from inner-shells other than s-levels, even require description by two partial waves rather than a single p-wave) make PD images intrinsically more complicated to interpret than X-ray and electron diffraction. More theoretical and experimental work is thus needed to develop a model that adequately includes the photoionization dynamics without requiring full-blown photoionization calculations, which are extremely difficult for larger molecules.

(ii) The need to align the gas-phase molecules with an extremely high degree of alignment in order not to wash out the fine angular interference structure, which is expected especially for higher photoelectron kinetic energies and for more complex molecules, requires some experimental improvements of existing alignment techniques. On the one hand, using photoelectron-ion coincidences to determine the orientation of the molecular axis works very well for many relatively small molecules, but becomes increasingly difficult for more complex molecules and for time-resolved studies, where a changing molecular structure shall be observed. On the other hand, laser-alignment techniques still struggle to achieve the necessary degree of alignment, and the strong laser fields that are present, e.g., during adiabatic alignment, can have unwanted effects on both the chemical dynamics and the molecular photoionization process.

(iii) In order to achieve the few-femtosecond temporal resolution that is needed to image many ultrafast reactions in molecules, the timing jitter between the femtosecond-laser-pump and the X-ray-probe pulse, which was, at the time of our measurements, the main practical limitation for the time-resolution in laser-pump FEL-probe

experiments[11], needs to be significantly reduced or, at least, to be compensated by shot-by-shot arrival-time measurements of both pulses.

(iv) Currently, the photon bandwidth of the FEL pulses, which is typically on the order of 0.2-1.0% for a SASE FEL[30,31], limits the theoretically achievable spatial resolution, since the existing monochromator beamlines typically either do not have sufficient transmission to allow, for dilute molecular targets, the count rates necessary to perform the experiments given the low repetition rates of the FELs, or they broaden the X-ray pulse length too much to allow experiments with few-femtosecond X-ray pulses.

In the following, we describe recent advances that address some of the above-mentioned challenges and that we plan to implement in our next fs-PD experiments:

(i) It has recently been shown that the use of multiple photoelectron energies in the region of 300 eV +/-150 eV may be more suitable to record photoelectron holograms of gas-phase molecules[29] than electron energies around 2 keV, as originally suggest by Krasniqi *et al.*[9], and that a description of the photoelectron scattering within the first Born approximation may already be valid for electron energies as low as 300 - 500 eV[32], which would facilitate the interpretation of the recorded photoelectron diffraction pattern in terms of a hologram. Electrons in this kinetic energy range are significantly easier to image with VMI spectrometers than 2 keV electrons, making such holography experiments less challenging from a purely technical point of view.

(ii) The rapid development of new and improved laser-alignment methods for gas-phase molecules suggests that future experiments will be able to achieve considerably higher degrees of alignment than we obtained in our previous FEL experiments. For example, it has been demonstrated that a degree of alignment of $<cos^2 \theta_{2D}> =$ 0.97 can be achieved by adiabatically laser-aligning iodobenzene molecules when an electrostatic deflector[33] is employed for selecting only the coldest molecules in the molecular beam[34]. Furthermore, it was recently demonstrated that a stretched femtosecond Ti:Sapphire laser pulse instead of a Nd:YAG laser pulse can be used to align carbonyl sulfide molecules to a very high degree[35], which would eliminate the limitation to a 30 Hz repetition rate in our experiments because of the Nd:YAG laser. Field-free alignment methods, which would allow pumping and probing the molecules at a time when the strong alignment-laser pulse is no longer present, have also recently achieved much improved degrees of alignment[36,37], suggesting that they may soon be a viable alternative to adiabatic laser alignment.

(iii) The limitations of the temporal resolution because of the arrival time jitter between the X-ray and the pump laser pulse have recently been improved dramatically by the development of cross-correlation tools at some FEL facilities[38,39,47], which allow correcting for this jitter in the data analysis such that the temporal resolution is, at present, mostly limited by the X-ray and laser pulse durations, as we have shown in recent time-resolved ion imaging experiment[40]. Other FEL facilities now operate laser-seeded FELs[41], which allows for much better intrinsic synchronization between the FEL and the femtosecond laser. This would, of course, also be the case when using a soft X-ray HHG source for a photoelectron diffraction experiment, making this a very promising avenue to achieve extremely high temporal resolution.

(iv) Seeded FELs (with laser seeding such as FERMI as well as with self-seeding, as recently demonstrated at LCLS[42]) also provide much narrower photon bandwidth, which addresses the above-mentioned limitation to the spatial resolution as well as allowing for high(er) resolution photoelectron spectroscopy in order to monitor, e.g., time-dependent changes of the electronic structure and of the core-level chemical shift in dissociating molecules.

Given these experimental and theoretical advances, our next FEL experiments, which are planned for the near future, will hopefully be another big step towards demonstrating femtosecond time-resolved fs-PD photoelectron diffraction and holography as a tool to image molecular structure during photochemical reactions. Performing such experiments using laser-based HHG sources, which are now starting to enter the photon energy range of typical inner-shell levels, would make the technique more widely accessible and would open up the possibility to achieve even better temporal resolution.

ACKNOWLEDGEMENTS

REFERENCES

[1] Fadley, C. S., "Diffraction and holography with photoelectrons and Auger electrons: some new directions," Surface Science Reports 19, 231–264 (1993).

[2] Woodruff, D. P. and Bradshaw, A. M., "Adsorbate structure determination on surfaces using photoelectron diffraction," Rep. Prog. Phys. 57, 1029 (1994).

[3] Fadley, C. S., "Atomic-level characterization of materials with core- and valence-level photoemission: basic phenomena and future directions," Surf. Interface Anal. 40, 1579–1605 (2008).

[4] Barton, J. J., "Photoelectron Holography," Phys. Rev. Lett. 61, 1356 (1988).

[5] Becker, U. Gessner, O. and Rüdel, A., "Photoelectron scattering in molecules and fullerenes," J. Electron Spectrosc. Relat. Phenom. 108, 189–201 (2000).

[6] Landers, A. et al., "Photoelectron Diffraction Mapping: Molecules Illuminated from Within," Phys. Rev. Lett. 87, 013002 (2001).

[7] Rolles, D., "Scattering and Coherence Phenomena in the Photoionization of Small Molecules, " PhD thesis, TU Berlin, Berlin (2005).

[8] Zimmermann, B. et al., "Localization and loss of coherence in molecular double-slit experiments," Nat. Phys. 4, 649–655 (2008).

[9] Krasniqi, F. Najjari, B. Strüder, L. Rolles, D. Voitkiv, A. and Ullrich J., "Imaging molecules from within: Ultrafast angström-scale structure determination of molecules via photoelectron holography using free-electron lasers," Phys. Rev. A 81, 033411 (2010).

[10] Boll R. et al., "Femtosecond Photoelectron Diffraction on Laser-Aligned Molecules: Towards Time-Resolved Imaging of Molecular Structure," Phys. Rev. A **88**, 061402(R) (2013).

[11] Rolles D. et al., "Femtosecond X-Ray Photoelectron Diffraction on Gas-Phase Dibromobenzene Molecules," J. Phys. B 47, 124035 (2014).

[12] Boll R. et al., "Imaging Molecular Structure through Femtosecond Photoelectron Diffraction on Aligned and Oriented Gas-Phase Molecules," Faraday Disc. 171, in press (2014); http://dx.doi.org/10.1039/C4FD00037D.

[13] Kazama, M., Fujikawa, T., Kishimoto, N., Mizuno, T. Adachi, J.-i., and Yagishita, A., "Photoelectron diffraction from single oriented molecules: Towards ultrafast structure determination of molecules using X-ray free-electron lasers," Physical Review A 87, 063417 (2013).

[14] Stener, M. and Decleva, P., private communication.

[15] Golovin A. V. et al., "Inner-shell photoelectron angular distributions from fixed-in-space OCS molecules: comparison between experiment and theory," J. Phys. B: At. Mol. Opt. Phys. 38, 3755 (2005).

[16] García de Abajo, F.J., Van Hove, M. A., and Fadley, C.S., "Multiple scattering of electrons in solids and molecules: A cluster-model approach," Phys. Rev. B 63, 075404 (2001).

[17] Díez Muiño, R., Rolles, D., García de Abajo, F. J., Fadley, C. S., and Van Hove, M.A., "Angular Distributions of Electrons Photoemitted from Core Levels of Oriented Diatomic Molecules: Multiple Scattering Theory in Non-Spherical Potentials," J. Phys. B 35, L359-L365 (2002).

[18] Reid K. L., "Photoelectron angular distributions," Annu. Rev. Phys. Chem. 54, 397 (2003).

[19] Stapelfeldt, H. and Seideman, T., "Aligning molecules with strong laser pulses," Rev. Mod. Phys., 2003, 75, 543.

[20] Strüder, L. et al.," Large-format, high-speed, X-ray pnCCDs combined with electron and ion imaging spectrometers in a multipurpose chamber for experiments at 4th generation light sources, " Nucl. Instrum. Methods Phys. Res. A 614, 483–96 (2010).

[21] Kazama, M. et al., "Theoretical study of X-ray photoelectron diffraction for fixed-in-space CO molecules," Chem. Phys. 373, 261 (2010).

[22] Meckel M. et al., "Laser-Induced Electron Tunneling and Diffraction," Science 320, 1478–82 (2008).

[23] Blaga C. I., Xu J., DiChiara A. D., Sistrunk E., Zhang K., Agostini P., Miller T. A., DiMauro L. F. and Lin C. D., "Imaging ultrafast molecular dynamics with laser-induced electron diffraction," Nature 483, 194 (2012).

[24] Küpper, J. et al., "X-Ray Diffraction from Isolated and Strongly Aligned Gas-Phase Molecules with a Free-Electron Laser," Phys. Rev. Lett. 112, 083002 (2014).

[25] Stern, S. et al., "Toward atomic resolution diffractive imaging of isolated molecules with X-ray free-electron lasers," Faraday Disc. 171, in press (2014); http://dx.doi.org/10.1039/c4fd00028e.

[26] Sciaini, G. and Miller, R. J. D., "Femtosecond electron diffraction: heralding the era of atomically resolved Dynamics," Rep. Prog. Phys. 74, 096101 (2011).

[27] Hensley, C., Yang, J., and Centurion, M., "Imaging of Isolated Molecules with Ultrafast Electron Pulses," Phys. Rev. Lett. 109, 133202 (2012).

[28] Gabor, D., "A New Microscopic Principle," Nature 161, 777 (1948).

[29] Sun, S. X.-L., Kaduwela, A. P., Gray, A. X., and Fadley, C. S., "Progress toward time-resolved molecular imaging: A theoretical study of optimal parameters in static photoelectron holography," Phys. Rev. A 89, 053415 (2014).

[30] Ackermann W. et al., "Operation of a free-electron laser from the extreme ultraviolet to the water window," Nature Photon. 1, 336 (2007).

[31] Emma P. et al., "First lasing and operation of an ångstrom-wavelength free-electron laser," Nature Photon. 4, 641 (2010).

[32] R. Boll, "Imaging Molecular Structure with Photoelectron Diffraction," PhD thesis, Heidelberg (2014); http://archiv.ub.uni-heidelberg.de/volltextserver/17103/.

[33] Filsinger, F. et al, "Pure Samples of Individual Conformers: The Separation of Stereoisomers of Complex Molecules Using Electric Fields," Angew. Chem. Int. Ed. 48, 6900 (2009).

[34] Holmegaard, L. et al., "Laser-Induced Alignment and Orientation of Quantum-State-Selected Large Molecules," Phys. Rev. Lett. 102, 023001 (2009).

[35] Trippel, S. et al., "Strongly driven quantum pendulum of the carbonyl sulfide molecule," Phys. Rev. A 89, 051401(R) (2014).

[36] Lee, K. F., Villeneuve, D. M., Corkum, P. B., Stolow, A., and Underwood, J. G., "Field-Free Three-Dimensional Alignment of Polyatomic Molecules," Phys. Rev. Lett. 97, 173001 (2006).

[37] Ren, X., Makhija, V., and Kumarappan, V. "Multipulse Three-Dimensional Alignment of Asymmetric Top Molecules," Phys. Rev. Lett. 112, 173602 (2014).

[38] Schorb, S. et al., "X-ray-optical cross correlator for gas-phase experiments at the LCLS free-electron laser," Appl. Phys. Lett. 100, 121107 (2012).

[39] Harmand, M. et al., "Achieving few-femtosecond time-sorting at hard X-ray free-electron lasers," Nature Photonics 7, 215 (2013).

[40] Erk, B. et al., "Imaging charge transfer in iodomethane upon x-ray photoabsorption," Science 345, 288 (2014).

[41] Allaria E. et al., "Highly coherent and stable pulses from the FERMI seeded free-electron laser in the extreme ultraviolet," Nature Photonics 6, 699-704 (2012).

[42] Amann J., et al., "Demonstration of self-seeding in a hard-X-ray free-electron laser," Nature Photonics 6, 693–698 (2012).

[43] NIST Electron Elastic-Scattering Cross-Section Database: Version 3.2 (2013); http://www.nist.gov/srd/nist64.cfm.

[44] Reid K L., "Photoelectron angular distributions: developments in applications to isolated molecular systems," Mol. Phys. 110, 131 (2012).

[45] Liebsch, A., "Theory of Angular Resolved Photoemission from Adsorbates," Phys. Rev. Lett. 32, 1203 (1974).

[46] Garcia, G. A., Nahon, L., and Powis, I., "Two-dimensional charged particle image inversion using a polar basis function expansion," Rev. Sci. Instr. 75, 4989 (2004).

[47] Hartmann, N. et al., "Sub-Femtosecond Precision Measurement of Relative X-Ray Arrival Time for Free-Electron Lasers," Nature Photonics 8, 706-709 (2014).